JOURNAL OF Applied Polymer SCIENCE

Capacitive Performance of Polyaniline/Manganese Dioxide Nanofiber Microsphere

Yu-Qiu Huo,[1] Shu-Bo Zhang,[1] Hai-Ying Zhang[1,2]

[1]Department of Chemistry, College of Science, Northeastern University, Shenyang 110819, People's Republic of China

[2]Sinopoly Tianjin New Energy Technology Co. Ltd, Tianjin 300480, People's Republic of China

Correspondence to: Y.-Q. Huo (E-mail: huoyuqiu@mail.neu.edu.cn)

ABSTRACT: This work has obtained polyaniline/manganese dioxide (PANI/MnO_2) nanofibers microsphere by interfacial chemical synthesis with 4-amino-thiophenol (4-ATP) as the structure-directing agent on the Au substrate. The cyclic voltammograms, galvanostatic charge–discharge, and electrochemical impedance spectroscopy were used to determine their capacitive performance. Powder X-ray diffraction, thermogravimetry and differential scanning calorimetry, Fourier transformed infrared spectroscopy, Brunauer–Emmett–Teller surface area measurements, and scanning electron microscope were performed for physical and chemical characterization. The effect of 4-ATP and acids on the capacitive performance of PANI/MnO_2 nanofibers microsphere was elucidated. The as-prepared PANI/MnO_2 was nanofiber about 30 nm diameters, and they further self-assembled into sphere. Its specific capacitance is up to 765 F g^{-1} at 1.0 mA cm^{-2} in 1.0*M* Na_2SO_4 solution. And it shows a high stability with a capacitance fade of only 14.9% after 400 charge–discharge cycles. The symmetric capacitor of PANI/MnO_2 (PM10+)/PANI/MnO_2 (PM10−) is assembled in 1.0*M* Na_2SO_4 solution, and its capacitive performance is compared with that of PANI (+)/PANI (−) and MnO_2 (+)/MnO_2 (−). © 2014 Wiley Periodicals, Inc. J. Appl. Polym. Sci. **2014**, *131*, 40575.

KEYWORDS: composites; conducting polymers; porous materials

Received 26 May 2013; accepted 7 February 2014

DOI: 10.1002/app.40575

INTRODUCTION

Due to comparatively higher power density and longer life cycle than secondary batteries and higher energy density compared with traditional capacitors, supercapacitors have gained much attention.[1] They are being widely used in digital communication, electric vehicles, intelligent instrument, and so on.[2–4] But more efforts are necessary to improve the performance of supercapacitor, especially the energy density and cycle stability. The performances of supercapacitors are determined by electrode materials.[5–7] Attractive electrode materials or structures are our ultimate purpose. The composite materials of conducting polymers and transition metal oxides have attracted considerable attention as they can combine the advantages of their separate components.[8–10] Polyaniline (PANI) is one candidate for supercapacitor due to its electrochemical reversibility, easy synthesis, high stability, good conductivity, and good stability.[11–13] But its resistance becomes larger and the capacity cycling performance deterioration due to the destruction of the polymer chain when used as electrode materials for electrochemical capacitors. Manganese oxide is a promising supercapacitor material due to its low cost, its environmental friendly characteristic, and its high theoretical specific capacitance. According to the Faraday reaction between manganese dioxide (MnO_2) and MnOOH, the theoretical specific capacitance of MnO_2 electrode can be approximately 1110 F g^{-1}.[14] However, the practical specific capacitance values of manganese oxides reported in the literature are much less than its theoretical value. Raymundo-Pinero et al.[15] found the specific capacitance of MnO_2 is between 150 and 250 F g^{-1}. Li et al.[16] have obtained the α-MnO_2 nanorod which delivered a maximum capacitance of 166.2 F g^{-1}. Devaraj and Munichandraiah[17] have also reported a SC value of 297 F g^{-1} for α-MnO_2 and 9 F g^{-1} for β-MnO_2. The addition of PANI can decrease the resistance of MnO_2, the combination of PANI and MnO_2 must benefit to the capacitive property of the MnO_2. Liu has obtained PANI-MnO_2 hybrid films by electropolymerization of aniline and electrodeposition of MnO_2 in the solution of aniline and $MnSO_4$. The hybrid film displays a specific capacitance value of 532 F g^{-1} at 2.4 mA cm^{-2} discharging current density.[18–20] Zhang has gained PANI-intercalated layered manganese oxide nanocomposite via exchange reaction of PANI with *n*-octadecyltrimethyl-ammonium intercalated manganese oxide in *N*-methyl-2-pyrrolidone solvent. Its maximum specific capacitance is 330 F g^{-1} at a constant current density of 1 A g^{-1}.[21] It is well known that the electrochemical properties of

material are significantly influenced by its dimensionality, morphology, and crystalline structure. The electrode material with a high surface area and a uniform, ordered pore network of nanometer dimension would be expected to exhibit superior performance in an electrochemical capacitor. In our previous work, PANI/MnO_x nanofiber microspheres were prepared by interfacial chemical synthesis with 4-amino-thiophenol (4-ATP) as the structure-directing agent on the Au substrate.[22] However, it is important to conduct a series of experiments before its practical applications. As a further research, the symmetric PANI/MnO_2 nanofiber microsphere capacitor PM10 (+)/PM10 (−) was assembled in 1.0*M* Na_2SO_4 solution in this article, and its capacitive performances were compared with that of PANI (+)/PANI (−) and MnO_2 (+)/MnO_2 (−). And some other factors, such as the role of 4-ATP in the forming of PANI/MnO_2 nanofiber microsphere, and the doping acids effect on their capacitive performance, are discussed in detail. Specially, the mechanism of 4-ATP inducing the formation of nanofiber microsphere were discussed. It is the first time to be mentioned. It proves that the PANI/MnO_2 nanofiber microspheres maintain the well capacitance performance even after assembled into capacitors. The power density of symmetric capacitor of PANI/MnO_2 (PM10+)/PANI/MnO_2 (PM10−) is 1248 W kg^{-1} in 1.0*M* Na_2SO_4 solution, which has enhanced 69% than that of MnO_2 (+)/MnO_2 (−). Its energy density approaches to 23 Wh kg^{-1}, which has improved 262% and 65% than that of PANI (+)/PANI(−) and MnO_2 (+)/MnO_2 (−), respectively.

EXPERIMENTAL

Pretreatment of the Au Substrate

The Au wires were first cleansed by immersion in an acetone solution for 0.5 h. After drying, the substrates were treated with a Piranha solution over 1 h at room temperature, with rigorous shaking. The Piranha solution was prepared by mixing three parts of H_2SO_4 and one part of H_2O_2 by volume at room temperature.[23] Following this, the substrates were rinsed with copious de-ionized water and then immersed into the 4-ATP/ethanol solution for more than 3 h under nitrogen condition. The 4-ATP/ethanol solutions contain 0.1, 0.5, 1.0, 1.5, 2.0, and 3.0 m*M* 4-ATP, respectively. The substrates were then rinsed with copious de-ionized water and ready for the subsequent application.

Preparation of PANI-MnO_2 Nanofiber Microsphere

Reagent-grade aniline was distilled under reduced pressure and the resulting colorless liquid was kept in the dark at room temperature before use. Other chemicals, such as 4-ATP and potassium permanganate, were analytic grade and used as previously received condition without any further treatment. All solutions were prepared from de-ionized water. A solution X comprising $KMnO_4$, HCl or H_2SO_4 or H_3PO_4, de-ionized water, and a solution Y comprising aniline, HCl or H_2SO_4 or H_3PO_4, and de-ionized water, were first prepared. The polymerization reaction was performed by pouring slowly 2.0 mL of solution Y atop 2.0 mL of solution X at ambient temperature without stirring for 4 h. The Au substrates were immersed in the surface of X solution during the polymerization reaction. After the reaction, the Au substrates were washed repeatedly with copious de-ionized water and ethanol, and then dried under ambient conditions. Loadings of the PANI/MnO_2 nanofiber microsphere were measured by the weight difference of the Au electrode before and after deposition, using Sartorius BT 25 S semimicrobalance with an accuracy of 0.01 mg. PANI/MnO_2 nanofiber microsphere electrodes were denoted as PM 01, PM 05, PM 10, PM 15, PM 20, and PM 30 respectively, according to the concentration of 4-ATP at the pretreatment of Au substrate. The PANI electrode was obtained under similar condition with 0.15*M* $(NH_4)_2S_2O_8$ instead of 0.15*M* $KMnO_4$ in X solution. And MnO_2 electrode is gained with 0.15*M* $MnSO_4$ instead of 0.15*M* aniline in Y solution.

Physical and Electrochemical Characterizations

The electrochemical characteristic of the PANI/MnO_2 nanofiber microsphere was performed using CHI660D electrochemical work station. All the experiments were performed within a three-electrode electrolytic cell. The PANI/MnO_2 nanofiber microsphere electrode was used as the working electrode, platinum foil (A = 1.0 cm^2) was used as the counter electrode and a saturated calomel electrode (SCE) was used as the reference electrodes. The cyclic voltammogram (CV) experiments were performed in a range of 0–0.9 V at a scan rate of 10 mV s^{-1}. The galvanostatic charge–discharge (CP) tests were performed in a potential window of 0–0.9 V at a current density of 1.0 mA cm^{-1} in 1.0*M* Na_2SO_4 solution. An amplitude rating of 5 mV within a frequency range from 40 kHz down to 1 Hz was used in electrochemical impedance spectroscopy measurements while the electrode was subjected to applied AC potentials of 0.05, 0.2, 0.4, 0.6, and 0.8 V, respectively. Symmetric capacitors of PANI/MnO_2 nanofiber microsphere, PANI, and MnO_2 were assembled by using the same kinds of electrodes as both negative and positive electrodes in 1.0*M* Na_2SO_4 solution.

The surface morphologies and chemical compositions of the PANI/MnO_2 nanofiber microspheres were examined with a scanning electron microscope (SEM, Shimadzu SSX550) and its auxiliary energy dispersive X-ray spectroscope (EDX). X-ray diffraction (XRD) pattern of PANI/MnO_2 nanofiber microspheres was obtained by exposing the sample to PW3040/60 powder XRD analysis with X-ray source of Cu Kα (0.15406 nm). The spectra were scanned in a range of 2θ = 10°–90°. Fourier transform infrared (FTIR, KBr) analysis was determined using Nicolet 510 PFT. Thermal behaviors of samples were examined by thermogravimetry and differential scanning calorimetry (TG-DSC) analysis were conducted on TGA/DSC 1 star^e system from room temperature up to 900°C at a heating ramp of 10°C min^{-1} in nitrogen. Brunauer–Emmett–Teller (BET) surface area measurements of the samples were performed using a TriStar II 3020 surface area analyzer after degassing overnight at around 200°C.

RESULTS AND DISCUSSION

Characterization of PANI/MnO_2 Nanofiber Microspheres

Figure 1 shows the XRD pattern of PM 10 (a) and MnO_2 (b). The broad peak located in the range of 15°–30° and centered at 2θ = 22° in Figure 1(a) is the characteristic peak of amorphous PANI with somewhat of a change in intensity and position.[24] The diffraction peaks appearing at about 38° and 65° are

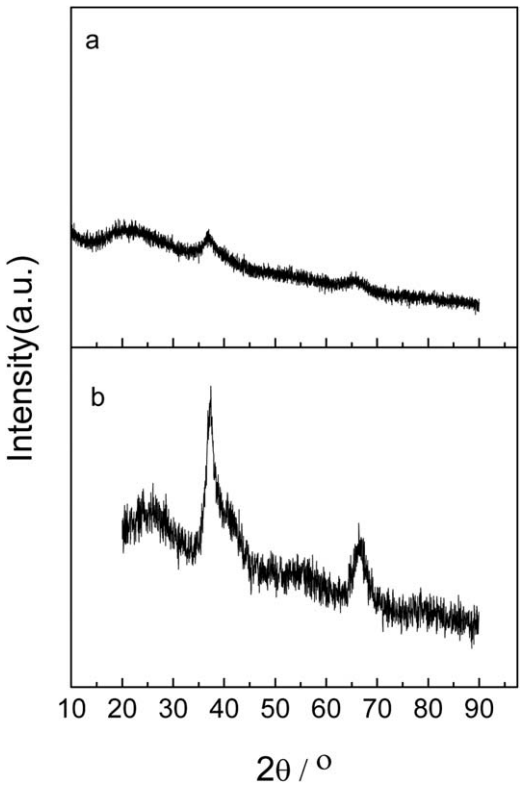

Figure 1. XRD pattern of PM 10 (a) and MnO_2 (b).

contributed to hydrate MnO_2,[25,26] which is coinciding with Figure 1(b). The attenuation of the diffraction peaks indicates that a part distortion in crystal structure of MnO_2 and transformation into amorphous phase has been occurred during the polymerization reaction.[27] It has been shown that the better electrochemical performance is obtained for the pseudocapacitor with oxide electrode containing higher amount of amorphous structure.[28] Such amorphous structure can cause the electrolyte to insert into the matrix easily leading to an increase in the reaction area between electrolyte and active electrode materials.[29]

To investigate the morphology of the sample on a large scale, it is characterized by SEM. Figure 2 displays the SEM images of PM 10 in different scales and its EDX analysis. It can be observed that the sample consists of nanofibers microsphere, in which nanofibers connect into chain-like structures with a large number of abnormity channels. The channels would benefit the transfer of proton and improve the capacitance behavior of PM 10.[30–33] This unique structure plays a more important role in improving the capacitance performance of PANI/MnO_2 than the simple hybrid of PANI and MnO_2. The EDX spectrum reveals PM 10 is composed of elements of Mn, O, C, and N. It should be noted that the Au peak is introduced (2.1 keV) by the coating of the sample before SEM and EDX tests. This further proves that both PANI and MnO_2 are introduced into PM 10. The BET results show that the specific surface area of

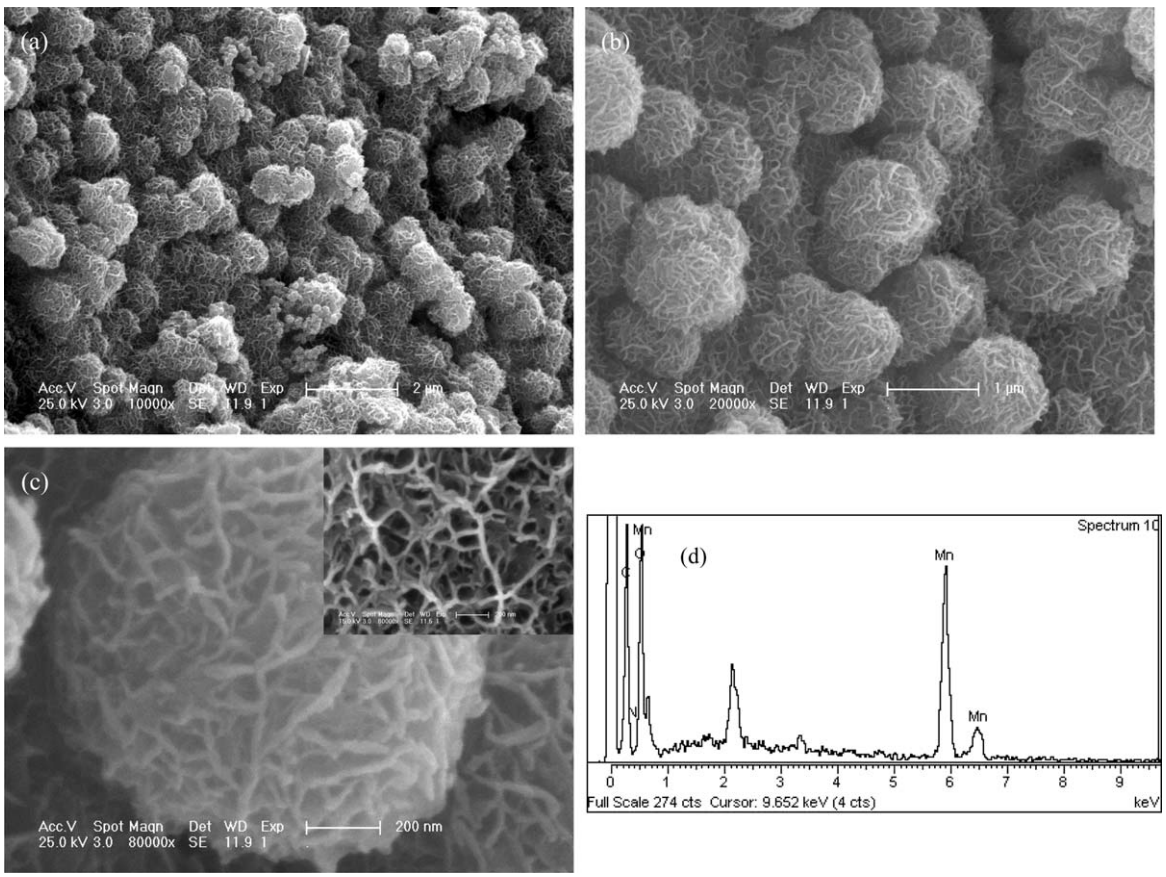

Figure 2. SEM images of PM 10 in different scales (a, b, c) and its EDX (d) pattern.

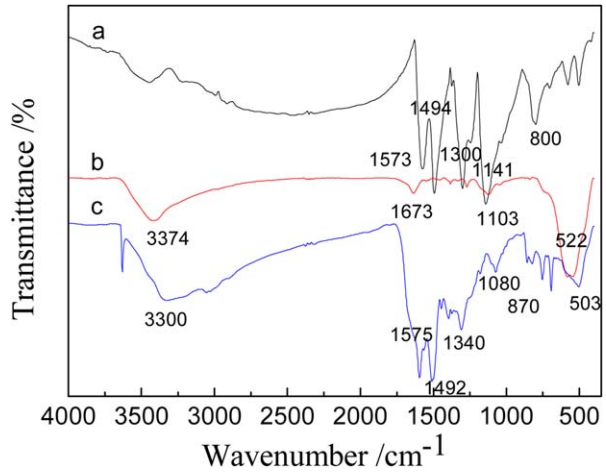

Figure 3. FTIR spectra of PANI (a), MnO_2 (b), and PM 10 (c). [Color figure can be viewed in the online issue, which is available at wileyonlinelibrary.com.]

PM 10 is 180 m^2 g^{-1}. It is at the same magnitude of the mesoporous materials.[34,35] This was confirmed by the SEM results.

Figure 3 displays the typical FTIR spectrum of the PANI (a), MnO_2 (b), and PM 10 (c). For Figure 3(a), the characteristic peaks at 1573 and 1494 cm^{-1} are owing to the stretching vibration of the quinoid ring and the benzenoid ring of PANI, respectively.[36,37] The absorption peak at 1300 cm^{-1} can be assigned to C—H stretching vibration with aromatic conjugation.[38] The band near 1141 cm^{-1} results from the N—Q—N (Q denotes quinoid ring) stretching mode and is an indication of electron delocalization in PANI.[40] The peak at 800 cm^{-1} is due to aromatic C—H out-of-plate deformation in1, 4-disubstituted benzene rings. At Figure 3(b), the broad band centers at about 3374 cm^{-1} is due to O—H of the chemically bonded water of MnO_2. The bands at 1673 and 1103 cm^{-1} are Mn—O—Mn stretching vibration band. The Mn—O bending vibration band of [MnO_6] octahedral appears at about 522 cm^{-1}. As shown in Figure 3(c), the broad band centers at 3300 cm^{-1} are due to O—H of the chemically bonded water of MnO_2 and N—H of PANI. The peaks at 1575 and 1492 cm^{-1} are assigned to the stretching vibration of the quinoid ring and the benzenoid ring of PANI, respectively. This is exactly coinciding with the results of PANI. The band at 1340 cm^{-1} can be assigned to C—H stretching vibration with aromatic conjugation.[38,39] The aromatic C—H out-of-plate deformation in 1, 4-disubstituted benzene rings locates at 870 cm^{-1}. The slight shift of the peaks shows the nature of PANI has changed due to the combination with MnO_2. The band at 1080 cm^{-1} is the Mn—O—Mn stretching vibration band. The Mn—O bending vibration band of [MnO_6] octahedral appears at about 503 cm^{-1}.[41,42] It can be seen that the structure of MnO_2 has also been changed due to the embedding of the PANI in the material. The above data indicate that PM 10 is a composite of PANI and MnO_2.

The TG-DSC curves of PANI (a), MnO_2 (b), and PM 10 (c) are shown in Figure 4. Figure 4(a) describes the decomposition process of PANI. One weight loss below 100°C is due to moisture in the sample. The other weight decrease at about 200°–400°C is due to the decomposition of PANI and the oxygen adsorption.[43–45] Figure 4(b) displays the thermal decomposition of MnO_2. The moisture of sample disappeared at 100°C. From 100°C to 200°C is the liberation of the chemically bonded water. The weight loss at 500°C is the decomposition of MnO_2 to O_2 and Mn_2O_3.[46,47] As shown in Figure 4(c), the initial weight loss corresponding to a broad endothermic peak is observed around 200°C for PM 10. It can be attributed to the loss of chemically bonded water in the samples.[48,49] It is corresponding with the FTIR results (Figure 3). Another weight decrease around 200°C–400°C is due to the decomposition of PANI and the oxygen adsorption. Oxygen adsorption should have slightly increased the weights, however, the decomposition of PANI would cut down the weights, and as a result the weight loss is small. The weight loss from 450°C to 550°C for the sample can be attributed to the decomposition of MnO_2 to O_2 and

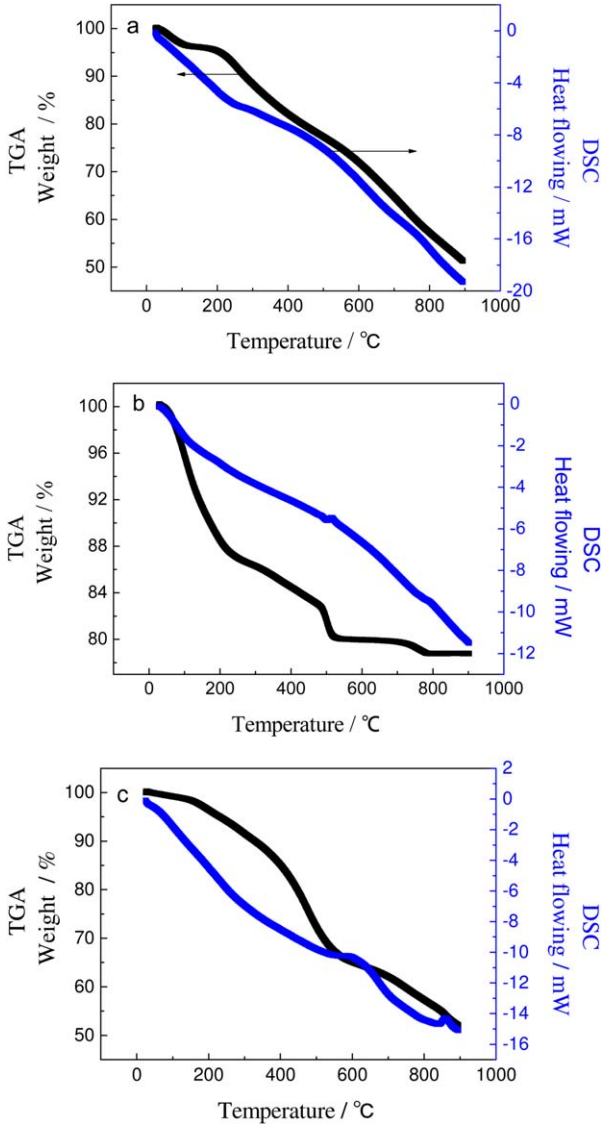

Figure 4. TG-DSC curves of PANI (a), MnO_2 (b), and PM 10 (c). [Color figure can be viewed in the online issue, which is available at wileyonlinelibrary.com.]

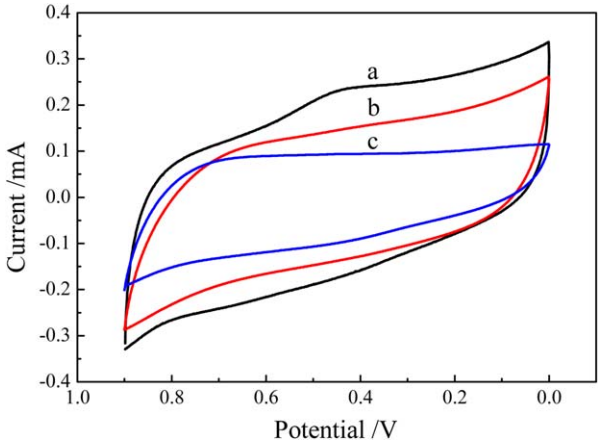

Figure 5. CVs of PANI/MnO_2 doped with different inorganic acids: (a) HCl, (b) H_2SO_4, and (c) H_3PO_4. Scan rate: 10 mV s^{-1}. [Color figure can be viewed in the online issue, which is available at wileyonlinelibrary.com.]

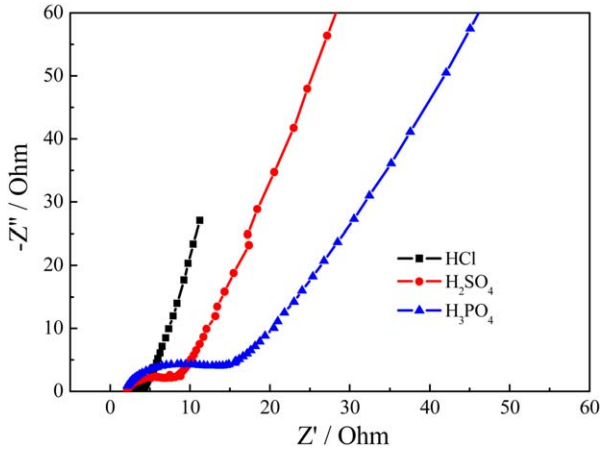

Figure 7. Impedance spectra in the range of 40 kHz to 1 Hz of the PANI/MnO_2 doping with different acids. [Color figure can be viewed in the online issue, which is available at wileyonlinelibrary.com.]

Mn_2O_3. The decomposition temperature of MnO_2 decreased slightly after mixture indicates that the addition of PANI effect the nature of MnO_2. These further confirm that the composite is not the simple mixture of PANI and MnO_2, these two ingredients has exactly interacted.

Doping Acids Influence on the Capacitive Performance of PANI/MnO_2 Nanofiber Microspheres

Keep the molar ratios of acid (HCl, H_2SO_4, and H_3PO_4) vs. aniline 1 : 1, the concentration of aniline is 0.15*M*, pH value is 4, the molar ratios of aniline/$KMnO_4$ is 1 : 1, the reaction time is 8 h, and the concentration of 4-ATP is 1.0 m*M*, the influence of acids on the capacitive performance of PANI/MnO_2 nanofiber microspheres were investigated. Figures 5 and 6 display the CVs and the galvanostatic CP curves of PANI/MnO_2 nanofiber microspheres obtained with different acids doping. The CV curves in Figure 5 all maintain a nearly rectangular shape and the potential responses during charge and discharge process in Figure 6 are nearly symmetrical. Both are characteristics of

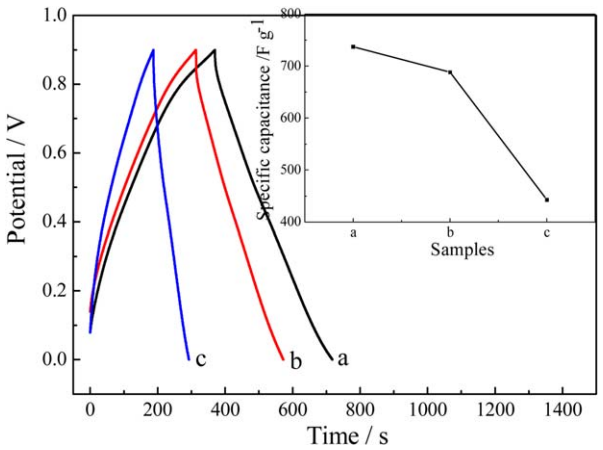

Figure 6. Charging–discharging curves of PANI/MnO_2 doped with different acids: HCl (a), H_2SO_4 (b), and H_3PO_4 (c) at 1 mA cm^{-2}. Inset shows the specific capacitances of samples. [Color figure can be viewed in the online issue, which is available at wileyonlinelibrary.com.]

excellent capacitance behavior and reversibility of these electrodes. But the CV curve area of PANI/MnO_2 nanofiber microspheres which doped with HCl is the largest among them. This illuminates that the doping of HCl would benefit the specific capacitance of PANI/MnO_2 nanofiber microspheres, which is approved by the inset of Figure 6. The specific capacitance of PANI/MnO_2 nanofiber microspheres doped with HCl is 737 F g^{-1}, while that doped with H_2SO_4 is 688 F g^{-1}, and that doped with H_3PO_4 is only 443 F g^{-1}. This result is in agreement with the work of Zhang et al. in which he discusses the effect of acid doping on the capacitance of PANI.[50] This phenomenon proved that the doping acids also take part in the conducting process of PANI/MnO_2 nanofiber microspheres. The little molecule could easily insert into the composite matrix, which will greatly impede the diffusion resistance and enhance the ion conductivity.

To give a further confirmation, the electrochemical impedance characteristics of the PANI/MnO_2 nanofiber microspheres doping with different acids are investigated at applied AC potential of 0.4 V within a frequency range from 40 kHz down to 1 Hz. The Nyquist diagrams are shown in Figure 7. The high frequency intercept of the semicircle with the real axis gives the internal resistance, including the resistance of the electrolyte, the intrinsic resistance of the active material, and the contact resistance at the interface active material/current collector. For these samples, the resistance of the electrolyte and the contact resistance at the interface active material/current collector are same. The internal resistances are determined by the intrinsic resistance of the active material. The PANI/MnO_2 nanofiber microspheres doping with HCl has the smallest internal resistance among them, which approves that HCl benefits the ion conductivity of the PANI/MnO_2 nanofiber microspheres. Furthermore, the semicircle in the high frequency region suggests that there is a charge transfer resistance (R_{ct}).[51] The PANI/MnO_2 nanofiber microspheres doping with HCl has the smallest R_{ct}. This means it is easy for the ion transfer between the solution and the electrode active center. So it shows the best electrochemical performance. A slope of a nearly vertical line arises in

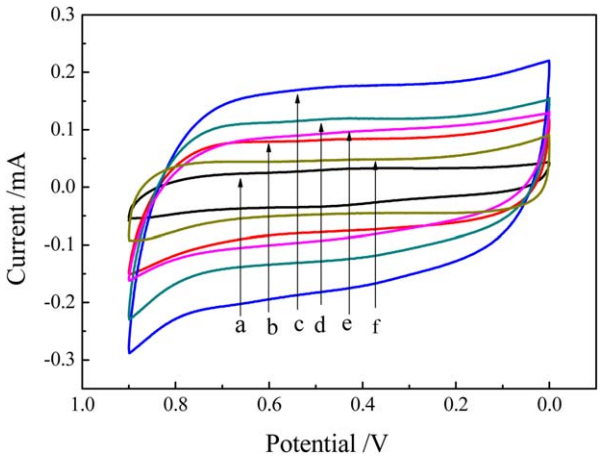

Figure 8. CVs of PM 01 (a), PM 05 (b), PM 10 (c), PM 15 (d), PM 20 (e), and PM 30 (f) in 1.0 mol L^{-1} Na_2SO_4. Scan rate: 10 mV s^{-1}. [Color figure can be viewed in the online issue, which is available at wileyonlinelibrary.com.]

the low frequency region on the curves due to the faradic pseudocapacitance of the electrode. The higher slope means the higher pseudocapacitive performance. So the sequence of the specific capacitance is PANI/MnO_2-HCl > PANI/MnO_2-H_2SO_4 > PAN/MnO_2-H_3PO_4, which is consistent with CV and CP results.

Relationship of 4-ATP Concentration on the Specific Capacitance of PANI/MnO_2 Nanofiber Microspheres

PANI/MnO_2 nanofiber microsphere samples were prepared with the concentration of 4-ATP is 0.1, 0.5, 1.0, 1.5, 2.0, and 3.0 m*M*, respectively, which were devoted as PM 01, PM 05, PM 10, PM 15, PM 20, and PM 30 in turn. The cyclic voltammetry of them at a scan rate of 10 mV s^{-1} in a potential range of 0 to 0.9 V (vs. SCE) in a 1.0*M* Na_2SO_4 solution is shown in Figure 8. It can be observed from Figure 8 that the CVs at whole potential range show rectangular mirror image, which mean these electrodes show ideal capacitive behavior and excellent reversibility.

The charging and discharging behaviors of them are examined by chronopotentiometry. Figure 9 plots the typical result from 0.0 to 0.9 V versus SCE in 1.0*M* Na_2SO_4 at the current density of 1 mA cm^{-2}. The charge curves are highly symmetric with the corresponding discharge counterparts over the entire potential region of the electrode. This means these electrodes possess of ideal capacitive behavior and excellent reversibility, which is consistent with the CV results. The specific capacitance is calculated from the CP curves by the eq. (1), where C_s is the specific capacitance based on the active materials,

$$C_s = \frac{it}{m(\Delta E)} \quad (1)$$

ΔE is the operating voltage of the cell, m is the mass of the active materials, and t is the discharge time obtained by chronopotentiometry. The values of C_s for the PM 01 (a), PM 05 (b), PM 10 (c), PM 15 (d), PM 20 (e), and PM 30 (f) are shown in inset of Figure 9. The C_s of PANI/MnO_2 nanofiber microspheres enhances with the increasing of 4-ATP concentration at first. It reaches the maximum value (765 F g^{-1}) when the concentration of 4-ATP is 1 m*M*. And then it decreases. This means that 4-ATP plays an important role in the capacitive properties of PANI/MnO_2 nanofiber microspheres. The schematic illustration of 4-ATP inducing the synthesis of PANI/MnO_2 nanofiber microsphene is shown in Figure 10. Figure 10(a) describes the micro structure and part B shows the macro patterns. 4-ATP, as a molecule containing SH group, can adsorb on the Au surface. And PANI/MnO_2 nanofibers can grow along its NH_2 group opposite SH group. If the concentration of 4-ATP is too low, it cannot form a uniform adsorption layer on the Au wires surface. However, if the concentration of 4-ATP is beyond its appropriate range, 4-ATP molecules would couple together and its single molecular adsorption layer would be destroyed also. PANI/MnO_2 would aggregate each other before the forming of nanofibers. Both of the above situations are disadvantage to the forming of PANI/MnO_2 nanofiber microspheres. Luckily 1 m*M* is suitable.

Cycling Stability of PANI/MnO_2 Nanofiber Microspheres

The cycling stability of the PM 10 is evaluated by CP test at a current density of 1.0 mA cm^{-2} for 400 cycles. The relationship of specific capacitance with the cycle times is shown in Figure 11. The inset is the initial 10 cycles. At the first stage, the specific capacitance only decrease slightly due to the relatively steady structure of the nanofiber microsphere. Then owing to the high frequency transfer of ions, the porous channel was collapsed, the capacitance performance decreased more than the former time. A capacitance fade of 14.9%, from 765 F g^{-1} to 651 F g^{-1}, is observed after 400 charge/discharge cycles, which is ascribed to the destruction of the nanofiber microspheres after 400 cycles.

EIS of PANI/MnO_2 Nanofiber Microspheres

Electrochemical impedance characteristics of the PM 10 were investigated at applied alternating voltage of 0.05, 0.20, 0.40, 0.60, and 0.80 V, respectively. The Nyquist diagrams in the range of 40 kHz to 1 Hz are shown in Figure 12. There is a

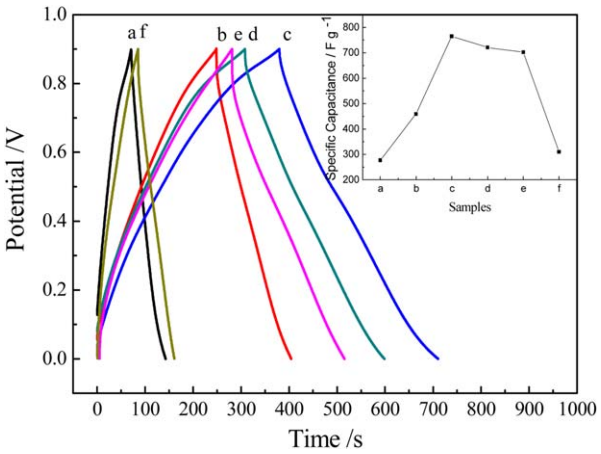

Figure 9. Charging–discharging curves of PM 01 (a), PM 05 (b), PM 10 (c), PM 15 (d), PM 20 (e), and PM 30 (f) in 1.0 mol L^{-1} Na_2SO_4, current density: 1 mA cm^{-2}. Inset is their specific capacitance. [Color figure can be viewed in the online issue, which is available at wileyonlinelibrary.com.]

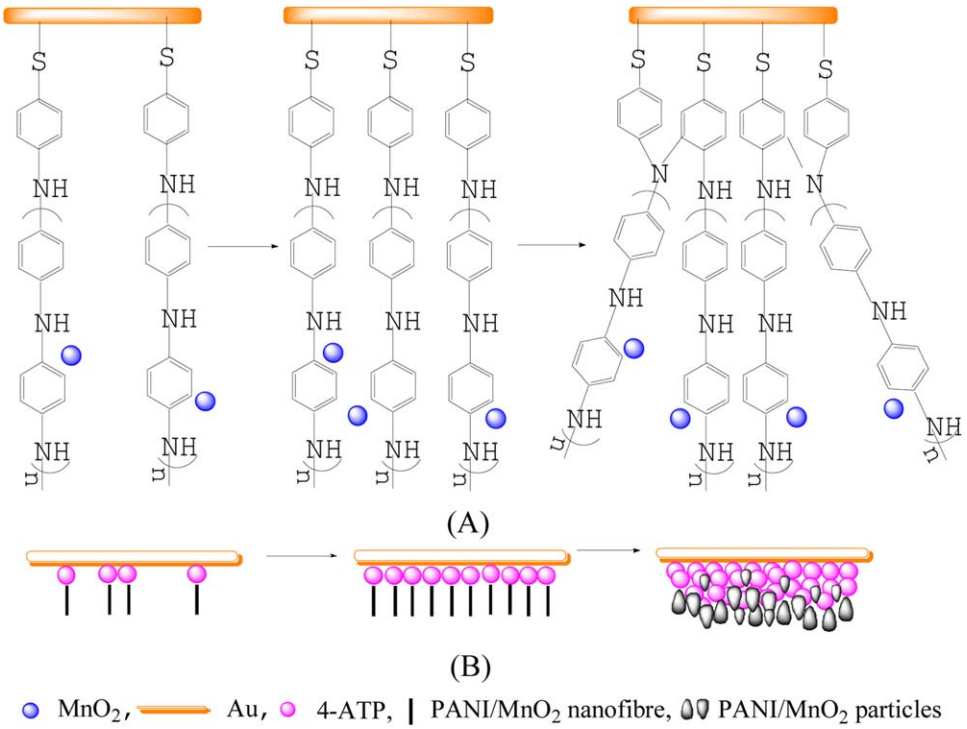

Figure 10. Schematic illustrations for the influence of 4-ATP concentration on the formation process of PANI/MnO_2 nanofiber. [Color figure can be viewed in the online issue, which is available at wileyonlinelibrary.com.]

semicircle impedance arc in the high frequency region on all the curves. This semicircle is attributable to the process at the electrode–electrolyte interface, which is expected to be the double-layer capacitance (C_{dl}) in parallel with the charge-transfer resistance (R_{ct}) due to the charge exchange and compensation at the electrode–electrolyte interface.[51] The semicircle radius of PM 10 reduced when the potential enhanced from 0.05 to 0.4 V, and then enlarged from 0.6 to 0.8 V. This indicates that PM 10 has the smallest Rct and best electrochemical performance at the potential of 0.4 V. It is further approved by the low frequency data. PM 10 had the largest slope at the potential of 0.4 V in the low frequency region. So PM 10 has the biggest specific capacitance at 0.4 V, which can be ascribed to the increased conductivity of the composite due to the formation of emeraldine at this potential. When the potential increased to 0.8 V, pernigraniline with poor conductivity became the most stable state of PANI, so the capacitive performance decreased.[52]

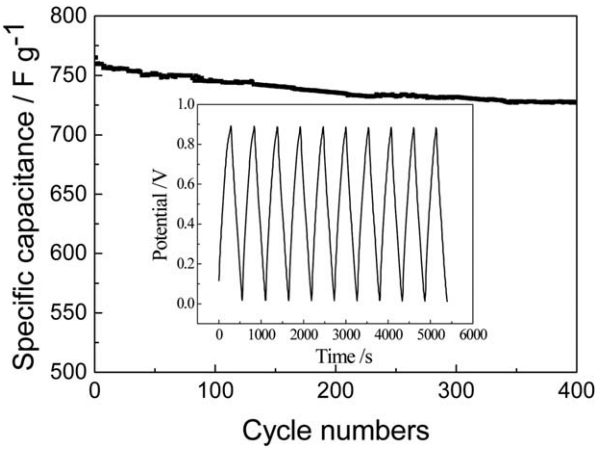

Figure 11. Relationship of specific capacitance with charging–discharging cycles. Inset is the initial 10 cycle's galvanostatic CP curves of the PM 10.

Symmetric Capacitor Performance of PANI/MnO_2 Nanofiber Microspheres

A symmetric PANI/MnO_2 nanofiber microspheres capacitor was assembled by using PM 10 electrodes as both positive and

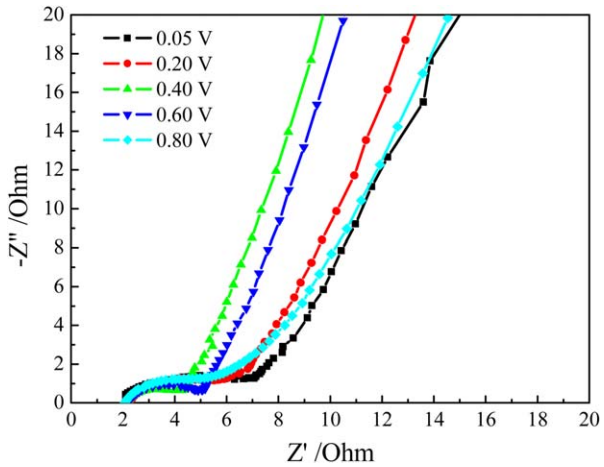

Figure 12. Impedance spectra in the range of 40 kHz to 1 Hz of PM 10 measured at different alternating voltage in 0.5 mol L^{-1} Na_2SO_4 solutions. [Color figure can be viewed in the online issue, which is available at wileyonlinelibrary.com.]

negative electrodes, with 1.0*M* Na_2SO_4 as the electrolyte. The specific capacitance (C_s) is calculated by the eq. (1). The energy density (E) is calculated by the eq. (2):

$$E = \frac{1}{2} C_s (\Delta E)^2 \quad (2)$$

The power density (P) is calculated by the eq. (3): whereΔE is the operating voltage of the capacitor; m is the total mass of the positive and negative electrode active material and t is the discharge time.

$$P = E/t \quad (3)$$

Under potential range of 0–0.9 V, the relationships of the specific capacitance, energy density, and power density of the symmetric PM10 (+)/PM10 (−) capacitor on the CP current density (1.0, 1.5, 2.0, 2.5, and 3.0 mA cm^{-2}) are displayed in Figure 13. The specific capacitance only decreased 15.8% (from 203 to 171 F g^{-1}) when the current density was enhanced from 1 to 3 mA cm^{-2}, meanwhile, the energy density reduced 15.8% (from 22.8 to 19.2 Wh kg^{-1}) and the power density increased 295.6% (from 1248 to 4937 W kg^{-1}). So it is a promising supercapacitor material for high power density and energy density. To compare, the symmetric PANI (+)/PANI (−) and MnO_2 (+)/MnO_2 (−) capacitors were also assembled with 1.0*M* Na_2SO_4 as the electrolyte. The galvanostatic CP curves, the specific capacitance, energy density, and power density of the symmetric PM10 (+)/PM10 (−), PANI (+)/PANI (−) and MnO_2 (+)/MnO_2 (−) capacitors at 1.0 mA cm^{-2} under potential range of 0–0.9 V are displayed in Figure 14. The potential responses during charge and discharge process are nearly symmetrical. They exhibit the excellent reversibility of these capacitors. The energy density of PM 10 (+)/PM 10 (−) capacitor was the highest among them. It has improved 262% and 65% than that of PANI (+)/PANI (−) and MnO_2 (+)/MnO_2 (−), respectively. Its power density is as high as 1248 W kg^{-1}, which has enhanced 69% than that of MnO_x (+)/MnO_x (−). This confirms that the combination of PANI and MnO_2 benefit the capacitance performance of the supercapacitors.

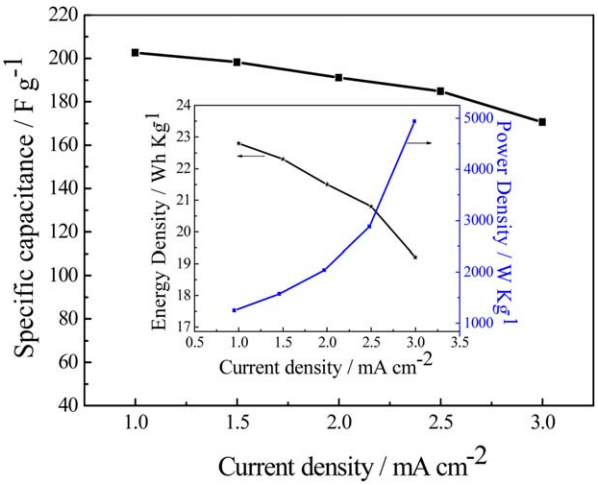

Figure 13. Dependence of specific capacitance on current densities of PM 10 symmetric capacitor. Inset is the relationship of energy density and power density of it on current density. [Color figure can be viewed in the online issue, which is available at wileyonlinelibrary.com.]

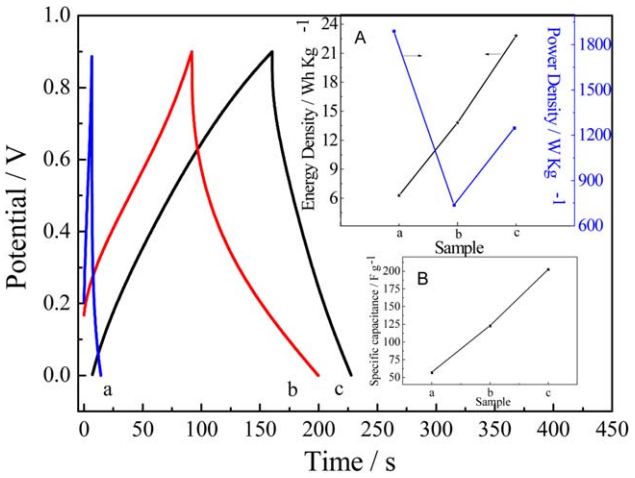

Figure 14. Charging–discharging curves of symmetric capacitors of PANI (a), MnO_2 (b), and PM 10 (c) in 0.5 mol L^{-1} Na_2SO_4 at 1 mA cm^{-2}. Inset A is their energy density and power density and inset B is their specific capacitance. [Color figure can be viewed in the online issue, which is available at wileyonlinelibrary.com.]

CONCLUSIONS

The concentration of 4-ATP by which the Au substrate is pretreated has a vital effect on the capacitive performance of PANI/MnO_2 nanofibers obtained by interfacial chemical synthesis on the Au substrate. The specific capacitance of PANI/MnO_2 nanofiber that obtained with 1 m*M* 4-ATP is 765 F g^{-1} at 1.0 mA cm^{-2} in 1.0*M* Na_2SO_4 solution. Its capacitance fades 14.9% after 400 times CP cycles. The power density of symmetric capacitor of PANI/MnO_2 (PM10+)/PANI/MnO_2 (PM10−) is 1248 W kg^{-1} in 1.0*M* Na_2SO_4 solution, which has enhanced 69% than that of MnO_2 (+)/MnO_2 (−). Its energy density approaches to 23 Wh kg^{-1}, which has improved 262% and 65% than that of PANI (+)/PANI (−) and MnO_2 (+)/MnO_2 (−), respectively. This confirms that PANI/MnO_2 nanofiber microsphere will be a promising supercapacitors material.

ACKNOWLEDGMENTS

This work was financially supported by the Fundamental Research Funds for the Central Universities of China (Grant No. N100405008).

REFERENCES

1. Conway, B. E. Electrochemical Supercapacitors, Scientific Fundamentals and Technological Applications; Kluwer Academic/Plenum Press: New York, **1999**.
2. Liu, F. J.; Hsu, T. F.; Yang, C. H. *J. Power Sources* **2009**, *191*, 678.
3. Chang, K. H.; Hu, C. C.; Huang, C. M.; Liu, Y. L.; Chang, C. I. *J. Power Sources* **2011**, *196*, 2387.
4. Zhang, D. C.; Zhang, X.; Chen, Y.; Yu, P.; Wang, C. H.; Ma, Y. W. *J. Power Sources* **2011**, *196*, 5990.
5. Hsieh, C. T.; Pan, C.; Chen, W. Y. *J. Power Sources* **2011**, *196*, 6055.

6. Zheng, J. P.; Cygan, P. J.; Jow, T. R. *J. Electrochem. Soc.* **1995**, *142*, 2699.
7. Devadas, A.; Baranton, S.; Napporn, T. W.; Coutanceau, C. *J. Power Sources* **2011**, *196*, 4044.
8. Liu, X. X.; Bian, L. J.; Zhang, L.; Zhang, L. J. *J. Solid State Electrochem.* **2007**, *11*, 1279.
9. Murugan, A. U.; Viswanath, A. K.; Gopinath, C. S. *J. Appl. Phys.* **2006**, *100*, 074319.
10. Abdiryim, T.; Ubul, A.; Jamal, R.; Tian, Y.; Awut, T.; Nurulla, I. *J. Appl. Polym. Sci.* **2012**, *126*, 697.
11. An, H. F.; Wang, Y.; Wang, X. Y.; Li, N.; Zheng, L. P. *J. Solid State Electrochem.* **2010**, *14*, 651.
12. Shaikh, S. F.; Lim, J.-Y.; Mane, R. S.; Zate, M. K.; Han, S.-H.; Joo, O.-S. *J. Appl. Polym. Sci.* **2013**, *128*, 3660.
13. Fonseca, C. P.; Almeida, D. A. L.; Baldan, M. R. *Chem. Phys. Lett.* **2011**, *511*, 73.
14. Pang, S. C.; Anderson, M. A.; Chapman, T. W. *J. Electrochem. Soc.* **2000**, *147*, 444.
15. Raymundo-Pinero, E.; Khomenko, V.; Frackowiak, E.; Beguin, F. *J. Electrochem. Soc.* **2005**, *152*, A229.
16. Li, Y.; Xie, H. Q.; Wang, J. F.; Chen, L. F. *Mater. Lett.* **2011**, *65*, 403.
17. Devaraj, S.; Munichandraiah, N. *J. Phys. Chem. C* **2008**, *112*, 4406.
18. Sun, L. J.; Liu, X. X.; Lau, K. K. T.; Chen, L.; Gu, W. M. *Electrochim. Acta* **2008**, *53*, 3036.
19. Sun, L. J.; Liu, X. X.; *Eur. Polym. J.* **2008**, *44*, 219.
20. Chen, L.; Sun, L. J.; Luan, F.; Liang, Y.; Li, Y.; Liu, X. X. *J. Power Sources* **2010**, *195*, 3742.
21. Zhang, X.; Ji, L. Y.; Zhang, S. C.; Yang, W. S. *J. Power Sources* **2007**, *173*, 1017.
22. Huo, Y. Q.; Zhang, H. Y.; Jiang, J. Y.; Yang, Y. *J. Mater. Sci.* **2012**, *47*, 7026.
23. Sun, Q. H.; Bi, W.; Fuller, T. F.; Ding, Y.; Deng, Y. L. *Macromol. Rapid Commun.* **2009**, *30*, 1027.
24. Rannou, P.; Nechtschein, M.; Travers, J. P.; Berner, D.; Woher, A.; Djurado, D. *Synth. Met.* **1999**, *101*, 734.
25. Ragupathy, P.; Vasan, H. N.; Munichandraiah, N. *J. Electrochem. Soc.* **2008**, *155*, A34.
26. Wei, W. F.; Cui, X. W.; Chen, W. X., Douglas, G. I. *Chem. Soc. Rev.* **2011**, *40*, 1697.
27. Li, J.; Cui, L.; Zhang, X. G. *Appl. Surf. Sci.* **2010**, *256*, 4339.
28. Chu, H. Y.; Lai, Q. Y.; Wang, L.; Lu, J. F.; Zhao, Y. *Ionics* **2010**, *16*, 233.
29. Hu, C. C.; Tsou, T. W. *J. Power Sources* **2003**, *115*, 179.
30. Hughes, M.; Shaffer, M. S. P.; Renouf, A. C.; Singh, C.; Chen, G. Z.; Fray, D. J.; Windle, A. H. *Adv. Mater.* **2002**, *14*, 382.
31. Zhang, H.; Cao, G. P.; Wang, Z. Y.; Yang, Y. S.; Shi, Z. J.; Gu, Z. N. *Electrochem. Commun.* **2008**, *10*, 1056.
32. Cao, Y. Y.; Mallouk, T. E. *Chem. Mater.* **2008**, *20*, 5260.
33. Lu, Z. Y.; Chang, Z.; Liu, J. F.; Sun, X. M. *Nano Res.* **2011**, *4*, 658.
34. Kim, D. S.; Jeon, J. D.; Shin, K. H. *Micropor. Mesopor. Mater.* **2013**, *181*, 61.
35. Yang, Z. H.; Pan, Y. M.; Mei, Z. S.; Zhang, W. X. *Appl. Surf. Sci.* **2012**, *258*, 4756.
36. Shi, X. Y.; Briseno, A. L.; Sanedrin, R. J.; Zhou, F. M. *Macromolecules* **2003**, *36*, 4093.
37. Dong, H.; Prasad, S.; Nyame, V.; Jones, W. E. *Chem. Mater.* **2004**, *16*, 371.
38. Pan, L. J.; Pu, L.; Shi, Y.; Sun, T.; Zhang, R.; Zheng, Y. D. *Adv. Funct. Mater.* **2006**, *16*, 1279.
39. Zeng, X. R.; Ko, T. M. *Polymers* **1998**, *39*, 1187.
40. Zhang, Z. M.; Deng, J. Y.; Shen, J. Y.; Wan, M. X.; Chen, Z. J. *Macromol. Rapid Commun.* **2007**, *28*, 585.
41. Tang, N. A.; Tian, X. K.; Yang, C.; Pi, Z. B.; Han, Q. *J. Phys. Chem. Solids* **2010**, *71*, 258.
42. Wang, H. E.; Qian, D. *Mater. Chem. Phys.* **2008**, *109*, 399.
43. Ragupathy, P.; Park, D. H.; Campet, G.; Vasan, H. N.; Hwang, S. J.; Choy, J. H.; Munichandraiah, N. *J. Phys. Chem. C* **2009**, *113*, 6303.
44. Martinez, M. L.; D'Amicis, F. A. L.; Beltramone, A. R.; Costa, M. B. G.; Anunziata, O. A. *Mater. Res. Bull.* **2011**, *46*, 1011.
45. Shao, L.; Qiu, J. H.; Liu, M. Z.; Feng, H. X.; Lei, L.; Zhang, G. H.; Zhao, Y.; Gao, C. M.; Qin, L. J. *Synth. Met.* **2011**, *161*, 806.
46. Ghaemi, M.; Ataherian, F.; Zolfaghari, A.; Jafari, S. M. *Electrochim. Acta* **2008**, *53*, 4607.
47. Ai, Z. H.; Zhang, L. Z.; Kong, F. H.; Liu, H.; Xing, W. T.; Qiu, J. R. *Mater. Chem. Phys.* **2008**, *111*, 162.
48. Wang, Y. T.; Lu, A. H.; Zhang, H. L.; Li, W. C. *J. Phys. Chem. C* **2011**, *115*, 5413.
49. Lu, Q.; Zhou, Y. K. *J. Power Sources* **2011**,*196*, 4088.
50. Zhang, Z. M.; Wei, Z. X.; Wan, M. X. *Macromolecules* **2002**, *35*, 5937.
51. Zhou, Y. K.; He, B. L.; Zhou, W. J.; Li, H. L. *J. Electrochem. Soc.* **2004**, *151*, A1052.
52. Patil, D. S.; Shaikh, J. S.; Dalavi, D. S.; Karanjkar, M. M.; Devan, R. S.; Ma, Y. R.; Patil, P. S. *J. Electrochem. Soc.* **2011**, *158*, A653.